

Fractal Morphology, Spatial Order, and Pore Structure in Microporous Membrane Filters

Luca Cipelletti, Marina Carpineti, and Marzio Giglio*

*Dipartimento di Fisica and Istituto Nazionale per la Fisica della Materia,
Università di Milano, Via Celoria 16, 20133 Milano, Italy*

Received July 25, 1996. In Final Form: October 14, 1996[Ⓞ]

We present a small-angle static light scattering study of some of the more commonly employed microporous membrane filters under quasi index matching conditions. We have investigated filters of various pore sizes and of two different chemical compositions, namely, acetate of cellulose (AC) and mixed esters of cellulose (MEC). The scattering data reveal that on short length scales the membranes have fractal morphology, a feature already reported in the literature for porous glasses. Membrane filters however exhibit a wider spectrum of morphologies. In fact, while AC filters may be described as surface fractals (like porous glasses), MEC membranes turn out to be mass fractals. Furthermore, for all the samples the scattered intensity distribution is peaked at a finite wave vector q_m , a feature typical of systems with a spatial quasi periodicity $\Lambda = 2\pi/q_m$. The relation between Λ and the pore size p_s depends on the type of membrane. In general Λ grows with p_s , but while for AC membranes Λ is roughly proportional to the pore size, for MEC filters a more complex behavior is observed. On the basis of these results and on mass density measurements we propose two different models for the AC and MEC membrane structure. The proposed picture is further supported by the observation of scanning microscope images.

I. Introduction

Microporous membrane filters are widely used in many scientific and technological applications, such as particle removal, microbiological and sterility testing, gas analysis, electrophoresis, and biological tissues simulation. Each membrane filter is characterized by a certain pore size value supplied by the manufacturers. The pore size p_s indicates the sieving capability of the filters; that is, it is a measure of the smallest particle that cannot flow through the membrane. The available pore sizes typically range from 0.025 to 8 μm , thus spanning over more than two decades. A wide variety of materials and manufacturing techniques are used in the membrane production. In particular, we focus our attention on membrane filters made of mixed esters of cellulose (MEC) and of acetate of cellulose (AC), both belonging to a large family of spongelike membranes, the typical thickness being about 150 μm .

We present for the first time a small-angle static light scattering study of these membranes. The filters have a white mat appearance, and in order to make light scattering measurements possible, all membranes were imbibed in a properly chosen solvent, to reduce the optical contrast to a convenient value. The technique gives a detailed picture of the membrane architecture. We find that at short length scales filters of both type exhibit a fractal nature. More in detail, AC membranes are porous solids with a fractal pore surface (surface fractals), while MEC membranes may be described as mass fractals. On larger scales, both kinds of filters show a certain degree of spatial order with a (quasi) periodicity Λ . To understand the relationship of the structure to the sieving capability, we studied the behavior of Λ as a function of p_s . We show that a relation between Λ and the pore size does exist, although it is not trivial and it is strongly dependent on the type of membrane. On the basis of scattering data and of mass density measurements we propose two different models for describing how the MEC and AC structure varies with the pore size. To further corroborate

the proposed picture, some scanning electron microscope measurements are also presented.

As a final point, we observe that both AC and MEC membranes exhibit many analogies with semirandom systems which have been extensively studied via small-angle scattering techniques, such as porous glasses^{1–3} or colloidal gels.^{4–6} In particular, AC filters have a structure reminiscent of spinodally decomposed materials such as porous glasses, while MEC membranes are morphologically similar to gels observed in the last stages of colloidal cluster aggregation. These analogies might be revealing of the processes actually employed in the fabrication of the filters.

The paper is organized as follows. In section II we briefly recall some properties of fractal objects and the main results that can be obtained with small-angle scattering. In section III we describe the sample preparation and the experimental setup. Finally, in section IV we present and discuss the experimental data.

II. Theory

In view of the discussion of the experimental data, we recall some basic results about fractal morphology and scattering from fractal objects.

A mass fractal is defined⁷ as an object such that the minimum number of cubes of edge l needed to cover it scales as

$$N(l) \propto l^{-d_m} \quad (1)$$

where $d_m \leq 3$ is the mass fractal dimension. In real

(1) Wiltzius, P.; Bates, F. S.; Dierker, S. B.; Wignall, G. D. *Phys. Rev. A* **1987**, *36*, 2991.

(2) Höhr, A.; Neumann, H.-B.; Schmidt, P. W.; Pfeifer, P.; Avnir, D. *Phys. Rev. B* **1988**, *38*, 1462.

(3) Levitz, P.; Ehret, G.; Sinha, S. K.; Drake, J. M. *J. Chem. Phys.* **1991**, *95*, 6151.

(4) Carpineti, M.; Giglio, M. *Phys. Rev. Lett.* **1992**, *68*, 3327.

(5) Bibette, J.; Mason, T. G.; Hu Gang; Weitz, D. A. *Phys. Rev. Lett.* **1992**, *69*, 981.

(6) Asnaghi, D.; Carpineti, M.; Giglio, M. *MRS Bull.* **1994**, *XIX*, 14.

(7) See, for example: Teixeira, J. In *On Growth and Form: Fractal and Non-Fractal Patterns in Physics*; Stanley, H. E., Ostrowsky, N., Eds.; Nijhoff: Boston, 1986; pp 154–155. Sinha, S. K. *Physica D* **1989**, *38*, 310. Pfeifer, P.; Obert, M. In *The Fractal Approach to Heterogeneous Chemistry*; Avnir, D., Ed.; Wiley: Chichester, England, 1989.

* Author to whom all correspondence should be addressed.
Electronic address: giglio@mi.infn.it.

Ⓞ Abstract published in *Advance ACS Abstracts*, December 1, 1996.

fractals, the scaling (1) holds only between two characteristic length ξ_1 and ξ_2 , the so called lower and upper cutoffs, respectively. The mass fractal dimension is usually not an integer, $d_m = 3$ being the limiting case of an ordinary solid. A fundamental quantity for describing the characteristic physical size of a fractal is the gyration radius $R_g = (\sum_i m_i r_i^2 / \sum_i m_i)^{1/2}$. We point out that, as a consequence of (1), the mass m of a fractal of radius R_g scales as $R_g^{d_m}$. Therefore, for a mass fractal with $d_m < 3$, the larger the gyration radius, the lower the density.

Fractal concepts may be also applied to self-similar surfaces. The surface fractal dimension d_s can be defined by the relation⁷

$$N(l) \propto l^{-d_s} \quad (2)$$

where $N(l)$ is the minimum number of squares of side l needed to cover the fractal surface. The surface fractal dimension varies from 2—the value for ordinary smooth surfaces—up to 3. Similarly to the case of mass fractals, for a real fractal surface eq 2 is valid for $\xi_1 < l < \xi_2$. We call a surface fractal⁷ a solid object ($d_m = 3$) bounded by a fractal surface.

Static light scattering is a very convenient tool to investigate fractal systems. In fact, for such systems the angular distribution of the scattered intensity $I(q)$ is given by

$$I(q) \propto q^{-\alpha} \quad (3)$$

where α is simply related to the fractal dimension, as will be seen in the following. In eq 3, $q = 4\pi n \lambda^{-1} \sin(\theta/2)$, n being the refractive index of the medium in which the scattering experiment is performed, λ the light vacuum wavelength, and θ the scattering angle. It is to be pointed out that eq 3 applies in the range $1/\xi_2 \ll q \ll 1/\xi_1$ (the condition $q \ll 1/\xi_1$ is usually fulfilled in the range of wave vectors accessible to small-angle light scattering experimental apparatus). As we mentioned above, the exponent α in the power law (3) is related to the fractal dimension. More in detail, for a mass fractal⁷

$$d_m = \alpha \quad (4a)$$

while for a surface fractal⁷

$$d_s = 6 - \alpha \quad (4b)$$

We note that in the case $d_s \rightarrow 2$ eq 3 together with eq 4b reduces to the well-known Porod's law $I(q) \propto q^{-4}$.

III. Materials and the Experimental Setup

We investigated both Millipore membrane filters made of mixed esters (nitrate and acetate) of cellulose (refractive index $n \cong 1.51^8$) and Sartorius membrane filters made of acetate of cellulose ($n \cong 1.47^9$), with pore size p_s ranging from 0.1 to 8 μm and from 0.2 to 8 μm , respectively.

To perform light scattering measurements, we placed each filter in a cuvette filled with a proper solvent. The solvent has been chosen for each sample in order to fully exploit the small-angle light scattering potentialities. On one hand, samples that scatter a considerable amount of light are requested. In fact, collecting light at very small angles has the disadvantage that spurious contributions due to stray light cannot be avoided. Therefore, one needs the scattered light to be at least a few percent of the incoming beam to have an acceptable signal to noise ratio. On the other hand, samples must not scatter too much in order to avoid multiple scattering effects. In particular, we typically

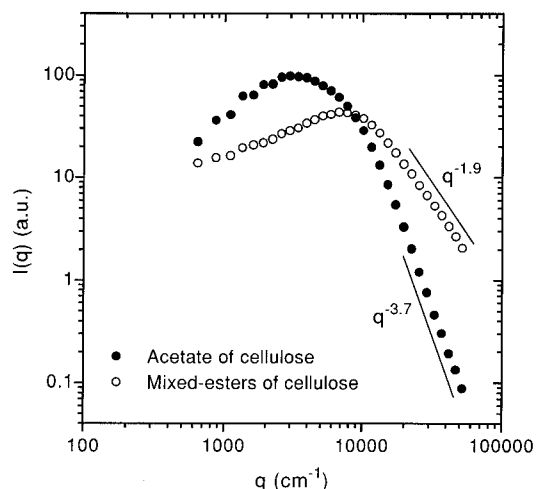


Figure 1. Intensity distributions of the light scattered by two membrane filters with the same pore size (1.2 μm) but different composition. Solid dots refer to the AC filter, open dots to the MEC filter. Both filters are imbibed in pure *p*-cymene.

worked with transmitted beam attenuations between 2% and 20%. To maintain the attenuation in the chosen range, the filters were imbibed in a proper mixture of *p*-cymene ($(\text{CH}_3)_2\text{CHC}_6\text{H}_4\text{-CH}_3$, refractive index $n^{20}_D = 1.490$) and 1-bromonaphthalene ($\text{C}_{10}\text{H}_7\text{Br}$, $n^{20}_D = 1.657$) with refractive index varying in the range $1.490 \leq n^{20}_D \leq 1.527$.

The major problem in sample preparation is the presence of trapped air bubbles, as they strongly scatter at low angle, thus producing a disturbing spurious signal. We therefore outgassed the membranes once they were placed in the matching fluid, and we used short ultrasound pulses to further improve air extraction. The outgassing procedure typically lasted a few hours, and it was stopped when no air bubble release could be detected by visual inspection.

The scattering data were recorded at room temperature with a small-angle static light scattering setup similar to the one described by Carpineti *et al.*¹⁰ We recall that the system allowed the collection of scattered light at 31 angles, corresponding to almost a two-decade range in transferred momentum q . Thanks to a slightly different optical configuration, we can now vary the accessible q range: all the MEC membrane scattering data were collected in the range $6 \times 10^2 \text{ cm}^{-1} \leq q \leq 5 \times 10^4 \text{ cm}^{-1}$, while AC membrane data were recorded either in the preceding transferred momentum range or in the $3 \times 10^2 \text{ cm}^{-1} \leq q \leq 3 \times 10^4 \text{ cm}^{-1}$ range.

IV. Experimental results and discussion

In Figure 1 we show the intensity distributions $I(q)$ of the light scattered by two membranes having the same pore size ($p_s = 1.2 \mu\text{m}$) but different chemical compositions, both imbibed in pure *p*-cymene. Although the two curves refer to the same value of p_s , they are quite noticeably different. We point out that their basic features are quite representative of the two types of membranes, as they have been observed for almost all the investigated pore sizes. In particular, we observe that for both samples the large q asymptotic behavior of the scattered light intensity follows the power law $I(q) \propto q^{-\alpha}$ (see eq 3) with $\alpha < 4$, and this reveals that both the membranes have fractal morphology on short length scale. Two different values of α have been measured depending on the membrane type, being $\alpha = 1.9$ for MEC membranes and $\alpha = 3.7$ for AC ones. As we mentioned in section II, these values of α reveal that great differences in the membrane morphologies do exist. In fact, for the MEC membranes $\alpha = 1.9$ indicates a mass fractal morphology with $d_m = \alpha$. By contrast $\alpha = 3.7$ reveals that AC membranes are surface

(8) Millipore technical brochure, Millipore Corp., Ashby R., Bedford, MA 01730.

(9) Sartorius technical brochure, Sartorius AG, P.O. Box 32 43, Weender Landstrasse 94-108, D-3400 Göttingen, Germany.

(10) Carpineti, M.; Ferri, F.; Giglio, M.; Paganini, E.; Perini, U. *Phys. Rev. A* **1990**, *42*, 7347.

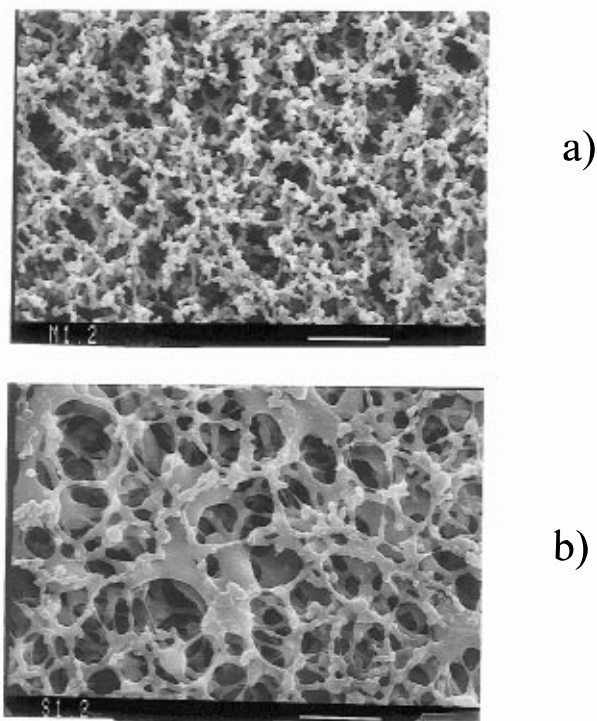


Figure 2. Scanning electron microscope images of a MEC (a) and an AC (b) filter, both with $p_s = 1.2 \mu\text{m}$. The bars refer to $10 \mu\text{m}$.

fractals, as the fractal morphology extends only to the boundary of the structure. From eq (4b) it follows that the surface fractal dimension d_s is $6 - \alpha = 2.3$.

Another fundamental feature which can be observed in Figure 1 is that the intensity distributions exhibit a peak at a finite wave vector q_m , a behavior typical of systems characterized by mass anticorrelation over a typical length scale $\Lambda = 2\pi/q_m$. The presence of a peak in the intensity distributions indicates that both membranes can be described as structures where each massive area has to be surrounded by a region where the probability of finding another massive domain is less than the average value. In other words there is a certain degree of spatial order with mass density fluctuations at a characteristic length Λ . It is also quite remarkable that, despite the fact that the pore size is the same ($p_s = 1.2 \mu\text{m}$), the peak positions are substantially different. The values of the characteristic length Λ that can be estimated for the two membranes are $\Lambda = 22.4 \mu\text{m}$ for the AC filter and $\Lambda = 8.4 \mu\text{m}$ for the MEC one. Both these values are quite far from the pore size ($1.2 \mu\text{m}$). To have qualitative evidence of the information obtained from the scattering data it is quite helpful to observe Figure 2, where two scanning electron microscope images of the same membranes of Figure 1 are shown. We observe that, although the two Figures are substantially different as a consequence of the different morphology of MEC (Figure 2a) and AC (Figure 2b) membranes, it can be appreciated that each structure exhibits a certain spatial regularity. In fact, both figures show that the void areas, surrounded by massive regions, are distributed in space quite uniformly. By visual inspection only, we cannot give a quantitative estimate of the typical length scale that can be associated with each membrane, but it can be easily observed that for the MEC membrane this length is definitely shorter than the one associated with the AC one. It turns out that light scattering is a very powerful technique with respect to direct observation. In fact, although the micrographs shown in Figure 2 provide detailed images of the mass spatial arrangement in the two different structures, light

scattering allows one to quantitatively estimate morphology and characteristic length of the two samples with a single measurement.

We point out that the peak-shaped intensity distribution shown in Figure 1 together with the fractal morphology is strongly reminiscent of other systems that have been studied in the past via small-angle scattering techniques. In particular, the light scattering distributions from MEC membranes are strongly similar to the ones observed for diffusion-limited colloidal aggregation in dense solutions.^{4,5} In fact, we recall that $d_m = 1.9$ is a typical mass fractal dimension reported for colloidal aggregation phenomena¹¹ and that the presence of a peak in the intensity distribution has been observed during the formation of colloidal gels, i.e. semirigid structures composed of interconnected fractal aggregates.⁴⁻⁶ By analogy we may model MEC membranes as a matrix of close packed mass fractal clusters, the average packing distance being equal to Λ . Incidentally, we point out that the electron microscope image shown in Figure 2a is strongly similar to images of colloidal gels obtained with a confocal microscope.¹² By contrast, AC membranes have a structure similar to porous materials obtained by etching a spinodally decomposed glass mixture, such as Vycor glass^{1-3,13} and other controlled-pore glasses^{2,14,15} which have been characterized via neutron and X-ray small-angle scattering. These materials have been found to exhibit a surface fractal nature, the surface fractal dimension being somewhere between 2.2 and 2.4. This value is indeed very close to that observed here for AC membrane filters. As a consequence, AC membrane filters may be modeled as spongelike porous solids. It is important to stress that it has been reported¹⁶ that some microporous membranes are produced via a phase separation process followed by the removal of one of the separated phases, a technique similar to that used to produce porous glasses. We point out that the similarities between the morphologies of the filters and that of the structures generated by the physical processes indicated above (colloidal cluster aggregation and spinodal decomposition) might be revealing of the manufacturing processes actually employed in the production of membrane filters.

In Figure 3 we present the scattered intensity versus q for AC membrane filters of different pore sizes. Similar data for the MEC filters are shown in Figure 4. The low q data for the smallest pore size membrane of both types are not shown since they are very noisy.¹⁷ We point out that the curves in Figure 4 have closely lying asymptotes at high q vectors, and for the largest pores the asymptotes are almost identical. This behavior is invariably observed in colloidal aggregation phenomena when there are no settling problems due to gravity. Indeed, it has been pointed out¹⁰ that this is a consequence of the conservation of the overall mass within the scattering volume. The same arguments used in ref 10 can be applied to MEC filters, as they can be modeled as close packed fractal

(11) Lin, M. Y.; Lindsay, H. M.; Weitz, D. A.; Ball, R. C.; Klein, R.; Meakin, P. *Nature* **1989**, *329*, 360. Lin, M. Y.; Lindsay, H. M.; Weitz, D. A.; Ball, R. C.; Klein, R.; Meakin, P. *J. Phys.: Condens. Matter* **1990**, *2*, 3093.

(12) Bremer, L. Ph.D. Thesis, Wageningen University (NL), 1992.

(13) Fratzl, P.; Vogl, G.; Klaumünzer, S. *J. Appl. Crystallogr.* **1991**, *24*, 588.

(14) Schmidt, P. W. *J. Appl. Crystallogr.* **1991**, *24*, 414.

(15) Kluijtmans, S. G. J. M.; Dhont, J. K. G.; Philipse, A. P. To be published.

(16) Meltzer, T. H. *Ultrapure Water* **1988**, July/August.

(17) All MEC filters and AC filters with $p_s \geq 0.8 \mu\text{m}$ are imbibed in pure *p*-cymene. For the smaller values of p_s of AC filters we slightly increased the optical mismatch by adding small amounts of 1-bromonaphthalene to the solvent to bring scattered signal to an adequate level, as small pore size membranes scatter less efficiently.

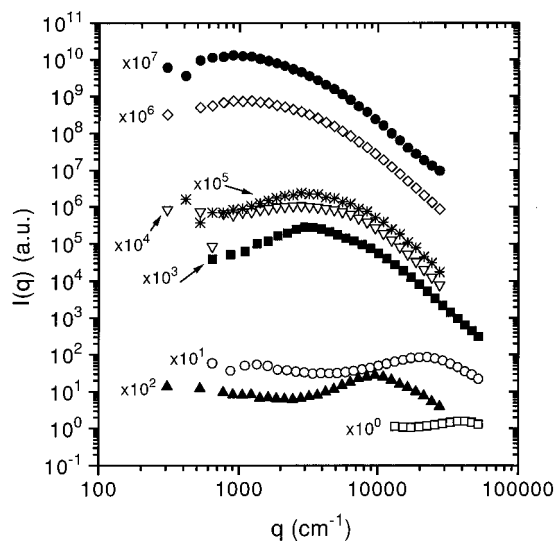


Figure 3. Scattered light intensity $I(q)$ for the AC membrane filters with pore size ranging from 0.2 to 8 μm : (\square) 0.2 μm ; (\circ) 0.45 μm ; (\blacktriangle) 0.64 μm ; (\blacksquare) 0.8 μm ; (∇) 1.2 μm ; ($*$) 3 μm ; (\diamond) 5 μm ; (\bullet) 8 μm . Large pore size membranes are imbibed in pure *p*-cymene, while for small pore size filters small amounts of 1-bromonaphthalene were added to the solvent to increase scattering efficiency. To avoid crowding the plot, the intensities of all points on each curve were multiplied by the factor indicated in the figure. The low q data of the 0.2 μm pore size membrane are not plotted, since they are very noisy.

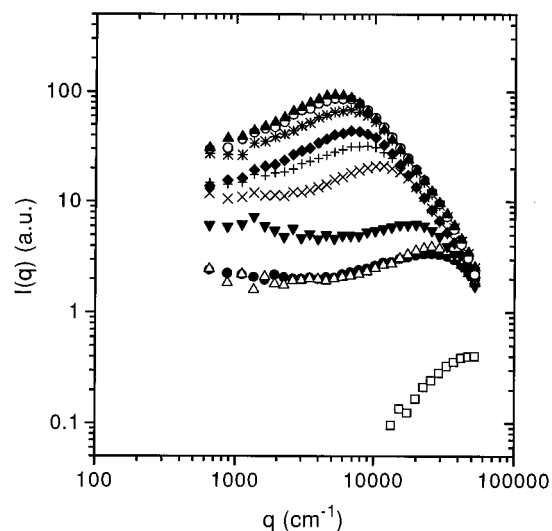


Figure 4. Scattered light intensity $I(q)$ for 10 MEC membrane filters, with pore size ranging from 0.1 to 8 μm : (\square) 0.1 μm ; (\bullet) 0.22 μm ; (\triangle) 0.3 μm ; (∇) 0.45 μm ; (\times) 0.64 μm ; ($+$) 0.8 μm ; (\blacklozenge) 1.2 μm ; ($*$) 3 μm ; (\circ) 5 μm ; (\blacktriangle) 8 μm . All membranes were imbibed in pure *p*-cymene. The low q data of the 0.1 μm pore size membrane are not plotted, since they are very noisy.

aggregates. This can be taken as an indication that the overall density of the filters does not change too much and for the largest pores is almost identical. This is consistent with the independent density measurements to be presented later for the MEC filters. Referring now to Figures 3 and 4, we observe that for both filter types each curve exhibits a peak and the peak position moves toward higher q values when p_s diminishes, eventually falling out of the instrumental range for the MEC membranes. This result suggests that Λ could be somehow related to the pore size. We point out that the existence of a relation between Λ and p_s is in principle not obvious. In fact, p_s is a measure of the membrane filter sieving capability, which is basically determined by the smallest size of the connections between the membrane voids that a particle is likely to go through

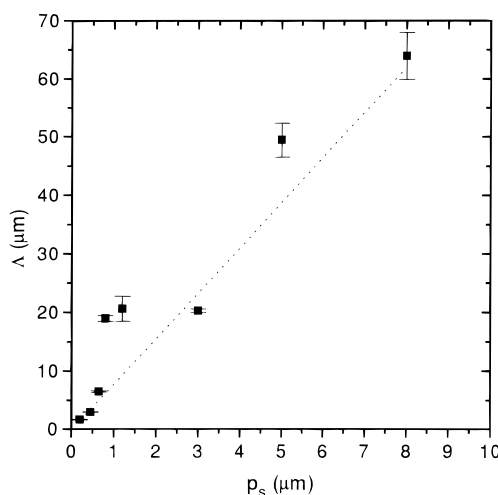


Figure 5. Pore size dependence of the mass density fluctuation length $\Lambda = 2\pi/q_m$ for the AC membrane filters. The dashed line is a linear fit through the origin over the whole range of rated pore sizes (the line is $\Lambda = \alpha p_s$ with $\alpha = 8.3$).

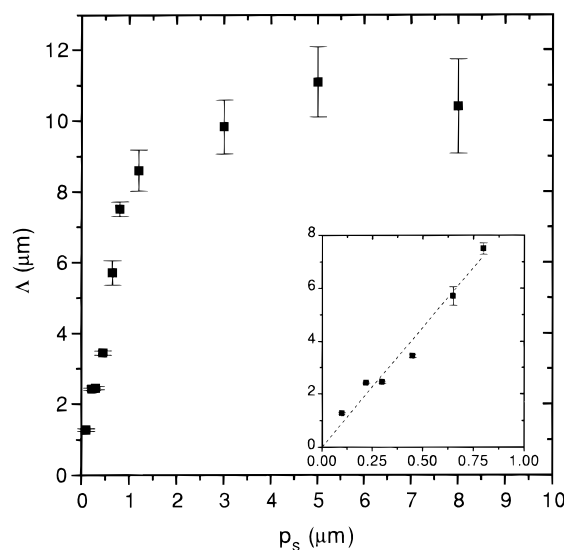


Figure 6. Pore size dependence of the mass density fluctuation length Λ for the MEC membrane filters. In the inset, the dashed line is a linear fit through the origin for $p_s \leq 0.8 \mu\text{m}$ (the line is $\Lambda = \alpha p_s$ with $\alpha = 9.0$).

during its travel across the filter. By contrast, Λ is only the typical mass density fluctuation length, and therefore it could be in principle independent of the size of the smallest path through the membrane. Furthermore, as Λ is by definition larger than the average size of the voids, Λ is expected to be only an upper limit for p_s , and therefore, membranes with different Λ may have the same pore size. We observe that this is exactly the case shown in Figure 1 and in Figure 2.

In Figure 5 and in Figure 6 the dependence of the characteristic length Λ on the pore size is plotted for AC and MEC membranes, respectively. It can easily be noticed that the two plots are appreciably different. For AC membranes, Λ varies roughly linearly with p_s in the whole range of pore sizes (the dashed line shows a linear fit through the origin of the data), and the typical mass density fluctuation length is always much larger than the pore size, the ratio Λ/p_s being approximately equal to 8.3. For MEC membranes two regions may be distinguished in the plot: for small pore sizes ($p_s < 1.2 \mu\text{m}$) the linear regime holds, and the typical mass density fluctuation length is approximately proportional to the pore size (see inset). Moreover, Λ is again much larger than p_s and Λ/p_s

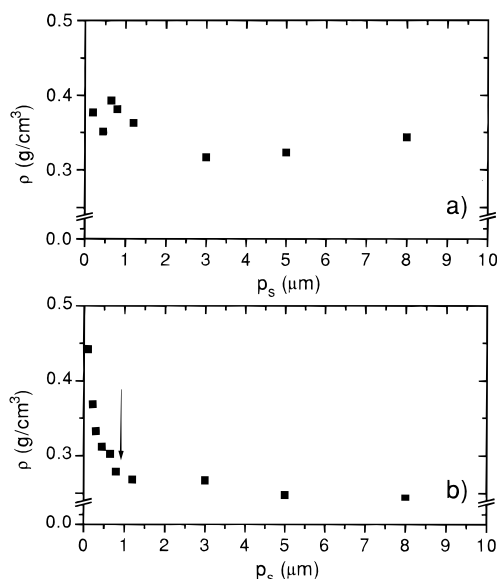


Figure 7. Membrane mass density as a function of the pore size: (a) AC membrane filters; (b) MEC membrane filters. Note in part b the two different ρ trends corresponding to the p_s ranges where the Λ linear behavior and the saturation regime are observed (see Figure 6). The arrow indicates where the transition from the linear to the saturation regime occurs.

= 9.0, a value similar to that observed for AC filters. By contrast, for larger p_s , Λ only slightly increases with p_s and eventually tends to saturate, reaching a value comparable to that of the pore size. Looking at Figure 4, we observe that for $p_s \geq 1.2 \mu\text{m}$ not only does the peak position hardly move but also the intensity distributions become quite similar and eventually tend to superimpose.

To better understand how the membrane structure changes with the pore size, we performed mass density measurements for different values of p_s . The results are shown in Figure 7, where the mass density ρ as a function of p_s is plotted for AC (a) and MEC membranes (b).¹⁸ We notice that for AC membranes the mass density ρ is approximately constant. Therefore both scattering and density data suggest that the morphology of the filters remains essentially the same as p_s changes, the scale of the structure varying accordingly. In other words, different sieving capabilities correspond to shrunk or dilated versions of the same pattern. In fact, due to the morphology of the AC membrane—a porous solid with fractal pore surfaces—if the structure is rescaled, the mass density should not change.¹⁹ By contrast, for MEC membranes there are two different trends corresponding to the two pore size ranges where the linear regime and the saturation regime of Λ are observed (see Figure 5). For $p_s < 1.2 \mu\text{m}$, where the ratio Λ/p_s is almost constant, ρ diminishes when p_s grows. At larger pore sizes, where Λ tends to saturate, strongly deviating from the linear regime, ρ does not appreciably change with p_s . By combining mass density and scattering data, we deduce that the scaling model proposed for AC membranes applies only to MEC filters with pore size less than $1.2 \mu\text{m}$. In fact, we recall that MEC membrane filters can be described as a matrix of close packed mass fractals of almost the same size. Consequently, a scale dilation of the structure not modifying the morphology necessarily implies a reduction

(18) Our mass density measurements are in very good agreement with Millipore data on the fraction of the sample volume occupied by the pores. Unfortunately, no similar data were available for the Sartorius membranes.

(19) See eq 2 and the following definition of a surface fractal in ref 14.

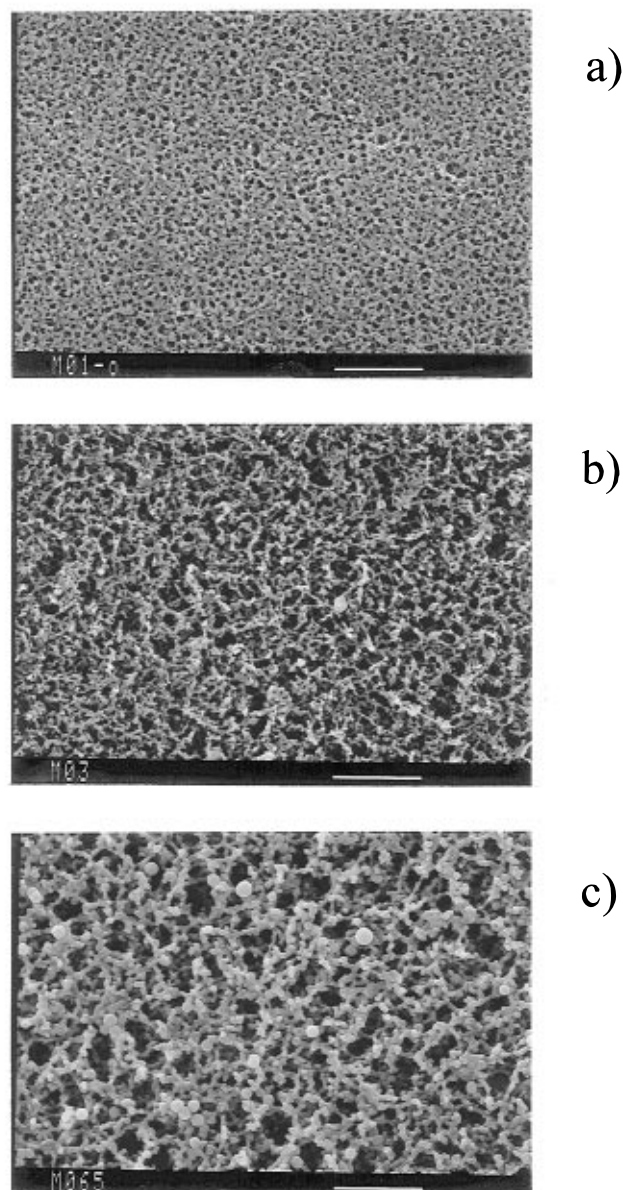
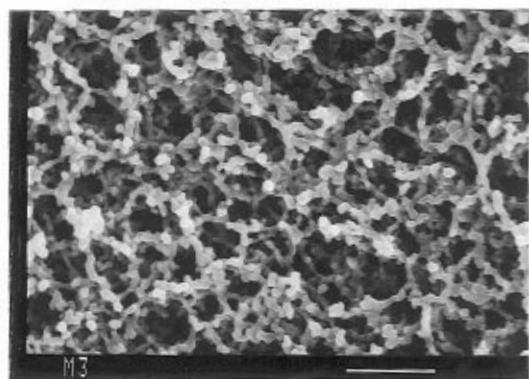


Figure 8. Micrographs of MEC membranes with pore size $0.1 \mu\text{m}$ (a), $0.3 \mu\text{m}$ (b), and $0.65 \mu\text{m}$ (c). The bars refer to $10 \mu\text{m}$.

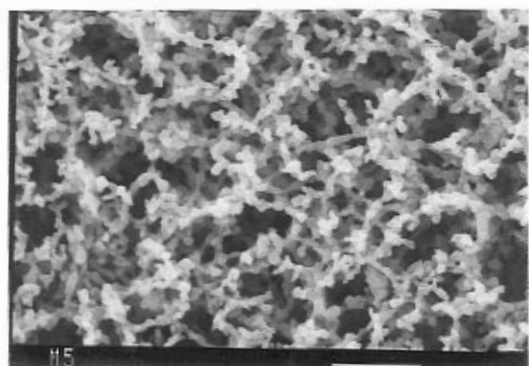
of the density ρ . In fact, the density of a fractal cluster of radius R_g scales as $R_g^{d_m-3}$, and the density ρ_m of a matrix of equally sized close packed fractal clusters behaves exactly as the density of one single cluster.²⁰ Therefore, as the size of the packed fractals of which the membrane is composed increases, the density of the membrane decreases, leading to the observed ρ trend.

In Figure 8 we present three micrographs of MEC membranes with pore sizes $0.1 \mu\text{m}$ (a), $0.3 \mu\text{m}$ (b), and $0.65 \mu\text{m}$ (c), for which we expect that an increase of the sieving capability implies a proportional dilation of the membrane structure. These images give an impressive, although only qualitative, demonstration of what has been inferred by light scattering and mass density measurements. In fact, the three micrographs show three substantially identical structures where the only difference seems to be the typical length scale, which increases with the pore size.

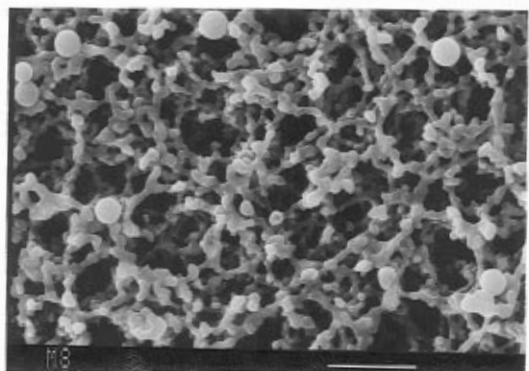
(20) The density ρ_m of a matrix of mass M_m and volume V_m of equally sized close packed fractals is $\rho_m = M_m/V_m = n_c M_c/V_m$, where n_c is the number of clusters of mass M_c and volume V_c contained in the matrix volume. But as $n_c \approx V_m/V_c$, it follows that $\rho_m \approx M_c/V_c = \rho_c$. This result is obviously quite general and does not depend on the clusters size.



a)



b)



c)

Figure 9. Micrographs of MEC membranes with pore size 3 μm (a), 5 μm (b), and 8 μm (c). The bars refer to 10 μm .

The case of MEC membranes with $p_s \geq 1.2 \mu\text{m}$ is more complex. In fact, the observation that Λ and ρ do not appreciably change with the pore size necessarily means that the structure of the membranes should be basically the same for filters with different p_s . The three micrographs shown in Figure 9a–c of MEC membranes with $p_s = 3, 5,$ and $8 \mu\text{m}$, respectively, give additional support to this picture. In fact, one can hardly notice appreciable differences between the three images.

The information obtained suggests the following picture for MEC filters with $p_s > 1.2 \mu\text{m}$. As almost identical structures give rise to different values of the pore size, the sieving capability should be determined by the presence (or absence) of very tenuous arms that adjust the size of the passages between the void areas. Although these arms heavily affect the sieving properties, and therefore p_s , they should be only an insignificant amount of the overall membrane mass, since they cannot be detected by mass density or scattering measurements and even by visual inspection.

V. Conclusions

We studied microporous membrane filters made of acetate and mixed esters of cellulose, by means of small-angle static light scattering. The data show that on a short length scale the membranes have fractal morphology, while at larger scales the system is characterized by a certain degree of spatial order, as is revealed by the presence of a peak at $q_m \neq 0$. Depending on the type, the membranes can be described either as a porous solid with fractal pore surface (AC filters) or as a network of close packed mass fractal clusters (MEC filters). The characteristic mass density fluctuation length $\Lambda = 2\pi/q_m$ is found to grow with the pore size, always being larger than it. For AC membranes, Λ is approximately proportional to p_s and the mass density ρ is constant over the whole range of pore sizes, suggesting that the membrane structure scales as p_s . MEC membranes show two different regimes. For small p_s , the scaling model is pertinent. In fact, Λ is proportional to the pore size, while the density decreases as p_s grows, as is to be expected for a material with mass fractal morphology. At large pore sizes, we believe that the overall membrane structure substantially does not vary, as indicated by light scattering and mass density measurements and scanning electron microscope images.

In conclusion, small-angle static light scattering, together with mass density measurements, has allowed the characterization of morphology and structure of a variety of microporous membrane filters. The results seem to indicate that small-angle static light scattering may be a promising, reasonably cheap tool for quality control for most membrane filters.

Acknowledgment. We thank D. A. Weitz for useful suggestions. We also wish to thank N. Ricci, A. Lombardo, and E. Paganini for the use of scanning electron microscope and cooperative assistance during the recording of the images. We are grateful to A. Riva and G. Rigamonti (Millipore S.p.A., Italy) for supplying some of the samples used in this work. This work has been supported by grants from the Ministero dell'Università e della Ricerca Scientifica e Tecnologica (MURST) and from the Comitato Nazionale Ricerche Tecnologiche e Innovazione of the Consiglio Nazionale delle Ricerche (CNR).

LA9607363